Serbian Tribology Society

SERBIATRIB '09

11th International Conference on Tribology

University of Belgrade Faculty of Mechanical Engineering

Belgrade, Serbia, 13 - 15 May 2009

THE EFFECT OF MICRO-BLASTING PROCEDURES ON THE CUTTING PERFORMANCE OF COATED TOOLS

K.-D. Bouzakis[1,3], G. Skordaris[1,3], S. Gerardis[1,3], G. Katirtzoglou[1,3], S. Makrimallakis[1,3], F. Klocke[2,3], E. Bouzakis[2]

[1] Laboratory for Machine Tools and Manufacturing Engineering, Mechanical Engineering Department, Aristoteles University of Thessaloniki, GR-54124, Greece

[2] Laboratory of Machine Tools and Production Engineering, Technical University of Aachen, Steinbachstr.53, D-52056 Aachen, Germany

[3]Fraunhofer Project Center Coatings in Manufacturing, in Centre for Research and Technology Hellas (CERTH) GR-57001 Thessaloniki, Greece and in Fraunhofer Institute for Production Technology (IPT) D-52074 Aachen, Germany

Abstract: *The conduct of micro-blasting on PVD films for improving the cutting performance of coated tools is often encountered in industry. In the present paper, the effect of micro-blasting procedures on film mechanical properties, cutting edge geometry and thus on tool life is introduced. A novel method for enabling the determination of coating strength properties gradation after micro-blasting was developed. Ball cratering tests were carried out at the flank and rake near the cutting edge to detect potential coating thickness change after micro-blasting. Moreover, the effect of micro-blasting conditions on the cutting edge geometry was examined by white light scanning and EDX microanalyses. The cutting performance of coated tools subjected to films' micro-blasting was investigated in milling. FEM supported calculations of the developed temperatures and stresses during material removal contributed for explaining the obtained tool wear results and herewith for optimizing the micro-blasting process.*

Keywords: *PVD coatings, micro-blasting, mechanical properties, cutting edge geometry, cutting performance*

1. INTRODUCTION

Micro-blasting on PVD films is an efficient method for increasing tool life of coated hardmetal tools [1,2,3]. The application of appropriate blasting conditions is of immense importance, since a superficial material deformation can be induced leading to mechanical properties increase [4]. Moreover, the cutting edge geometry might be changed after micro-blasting at various conditions, caused by abrasion. These potential effects of micro-blasting on coatings are demonstrated in figure 1. The knowledge of the related mechanisms is pivotal, since both can significantly affect the cutting performance [5].

In the paper, a method is introduced for determining film strength properties stratification versus the coating thickness after micro-blasting. On one hand, this method is based on a developed FEM-based simulation of the penetration of a blasting grain into the coating material, and on the other hand on nanoindentations and on X-ray diffraction (XRD) measurements. Furthermore, appropriate experimental and analytical investigations were conducted providing insight concerning the effect of blasting parameters on film distribution along the cutting edge. The wear behaviour of coated and variously micro-blasted tools was investigated in milling.

The TiAlN films, with an Al/Ti ratio equal to 60/40, were manufactured by a CEMECON C9000 coating machine. The film thickness was approximately 3 μm. A PVD process technology with high ionization sputtering and pulsing (HIS and HIP) was applied, leading to nano-structured, nano-laminated and nano-dispersed coating systems

[6]. The nanoindentations were carried out by a FISCHERSCOPE H100 device. The residual stresses of the films were measured by X-ray

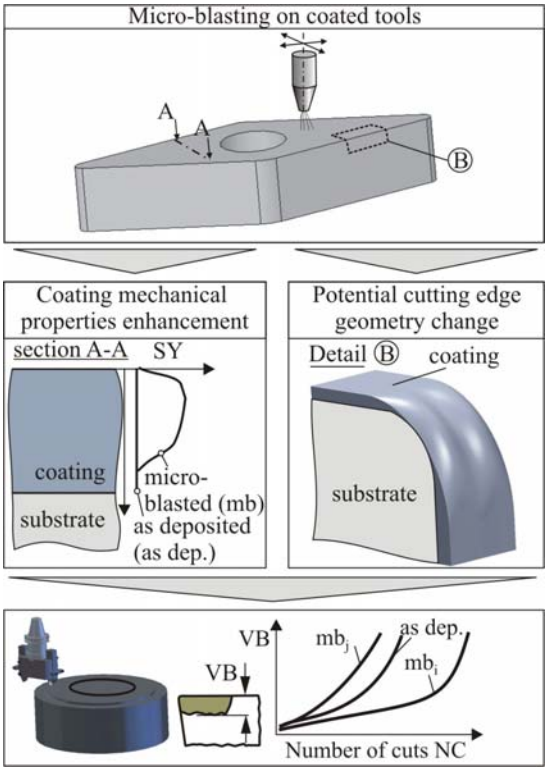

Figure 1. Coatings' micro-blasting effects.

diffraction technique, particularly through the $\sin^2\psi$ method at a certain depth from the film surface [1]. The used device was a SEIFERT XRD 3000 unit, equipped with a 4-circle goniometer. The white light scanning (confocal) 3D measurements system μSURF of NANOFOCUS AG was applied to capture cutting edge radius and coating thickness

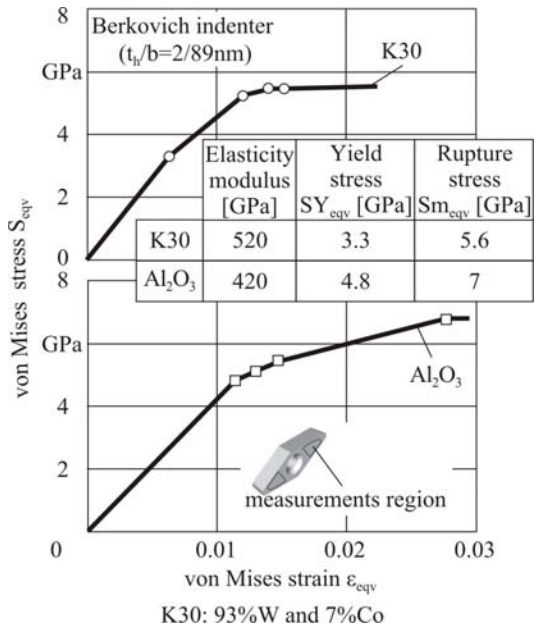

Figure 2. Substrate's and micro-blasting grains' strength properties.

distributions. The used Scanning Electron Microscope (SEM) was a Joel JSM-840. EDX microanalyses were also conducted by this device. The developed thermal and mechanical loads during the material removal process were determined by FEM-calculations, using the DEFORM [7] and ANSYS [8] software packages.

2. SUBSTRATE, COATING AND MICRO-BLASTING GRAINS MATERIALS CHARACTERIZATION

2.1 Determination of substrate and micro-blasting grains mechanical properties

The applied substrates are cemented carbides (hardmetals) inserts of K30 quality, with chemical composition of approximately 93% W and 7% Co. The substrate's mechanical properties as well as the corresponding ones of the Al_2O_3 grains used in micro-blasting of the examined TiAlN films are exhibited in figure 2. These data were obtained by evaluation of nanoindentation results, applying methods introduced in [9]. The determined hardmetal properties are valid for the entire insert structure, since a superficial strength increase

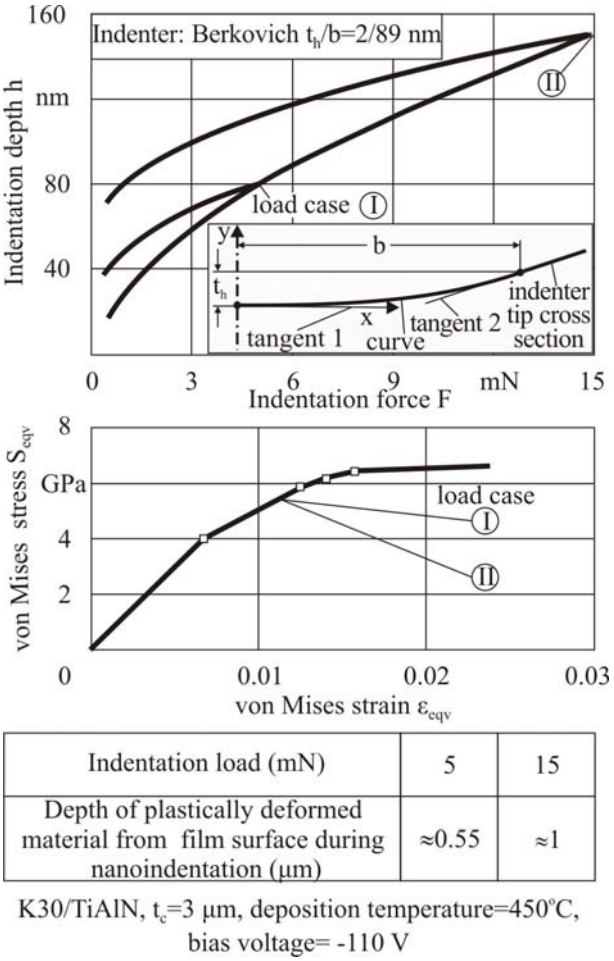

Indentation load (mN)	5	15
Depth of plastically deformed material from film surface during nanoindentation (μm)	≈0.55	≈1

K30/TiAlN, t_c=3 μm, deposition temperature=450°C, bias voltage= -110 V

Figure 3. Nanoindentation results at various depths and strength properties in the as deposited coating.

through micro-blasting before the film deposition to improve the coating adhesion is revoked during the PVD process due to annealing [10]. The attained data are considered in the FEM-simulation of the grain penetration into the coating.

2.2 Determination of coating mechanical properties before micro-blasting

To check whether a superficial strength properties gradation in the as deposited TiAlN film surfaces exists, nanoindentations at loads of 5 and 15 mN were conducted; the corresponding results are presented in the upper part of figure 3. The obtained data from every nanoindentation case were evaluated by the "SSCUBONI" algorithm [9] and the related coating's material constitutive laws

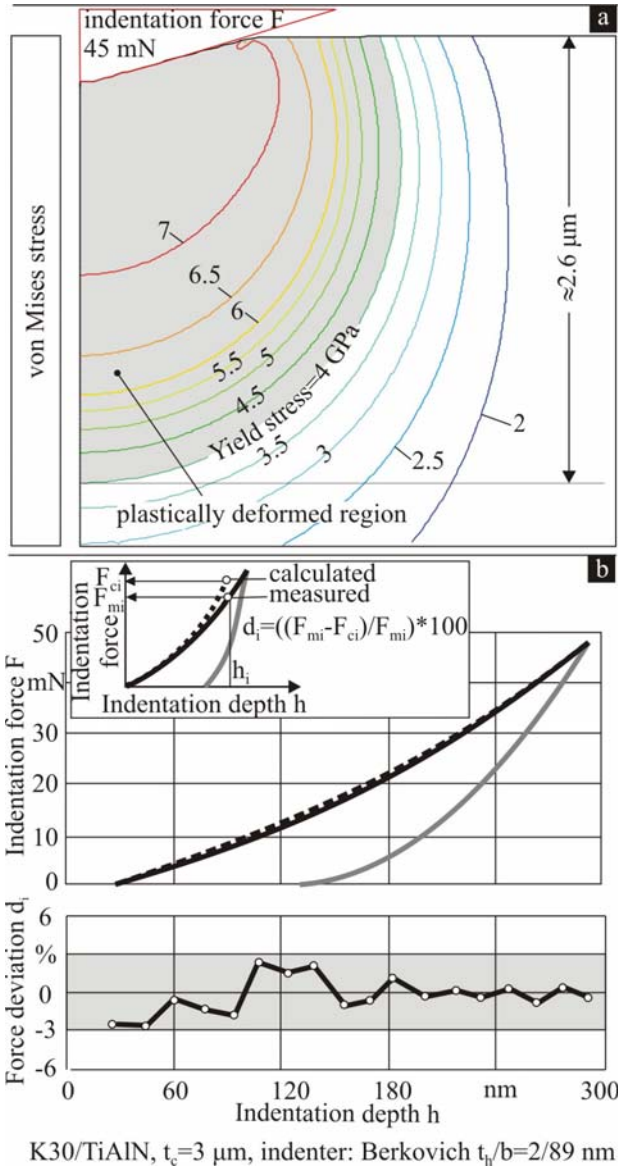

Figure 4. a. Occurring von Mises stress field in the as deposited film case during nanoindentation at a large indentation load. b. Deviations between measured and calculated nanoindentation forces versus the penetration depth, in the case of the as deposited TiAlN coating.

were determined. In both cases practically the same stress-strain curve occurred, as illustrated in the lower part of figure 3.

Furthermore, to test the validity of the determined film mechanical properties and to describe the coating material deformation at larger depths from the film surface, nanoindentations were carried out at an increased indentation force of 45 mN. As it is demonstrated in figure 4a, the coating material is loaded over the film yield stress, in the shaded area, up to a larger depth of approximately 2.6 µm compared to ca. 0.55 and 1 µm at the indentation loads of 5 and 15 mN, respectively (see figure 3). The measured course of the indentation depth versus the indentation force during loading was compared to the corresponding determined one, by the FEM-based simulation of nanoindentation. In these calculations, stress-strain data were employed, associated to film regions closer to the coating surface, i.e. detected at the lower indentation loads of 5 and 15 mN, as depicted in figure 3. The resulting force deviations d_i between measured and calculated indentation forces versus the indentation depth during loading are exhibited in the bottom part of figure 4b. The force deviations are less than ±3%. In this way, the applied coating strength properties versus the film thickness after the physical vapour deposition, at least up to a depth from the film surface of ca. 2.6 µm can be considered as unique. The used high ionization sputtering (HIS) and high ionization pulsing (HIP) during the PVD process [6] contributed to the achievement of a fine coating structure and herewith to the unique mechanical properties. This effect was theoretically explained by molecular dynamic calculations of the typical evolving microstructure for different energies of the adatoms during PVD processes [11].

2.3 Determination of coating mechanical properties after micro-blasting at various pressures

Cemented carbides inserts coated with the described TiAlN films were micro-blasted at the pressures of 0.2, 0.4 and 0.6 MPa. The micro-blasting time of four seconds was held constant in all conducted investigations. Over this time, at the applied micro-blasting conditions, no significant effect on the nanoindentation results and on the residual stresses was detected [1]. The related process conditions are monitored in figure 5. Nanoindentations were conducted in all the examined micro-blasted film cases at a maximum load of 5 mN, as shown in the upper diagram of the same figure. It is obvious that micro-blasting on

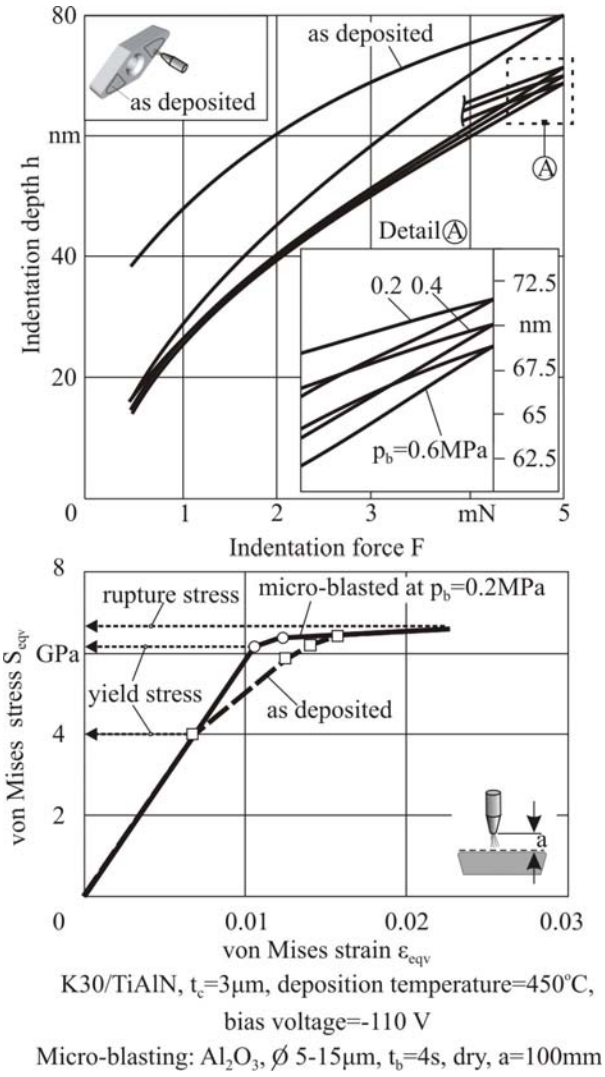

Figure 5. Nanoindentation results on TiAlN coatings after micro-blasting at various pressures and related film stress-strain curves.

PVD films leads to a significant decrease of the maximum indentation depth. These results were evaluated by the method described in [9] and the superficial elasto-plastic film properties were determined. The calculated stress strain curve at the micro-blasting pressure of 0.2 MPa is displayed in the diagram at the bottom figure part. In the same diagram, the stress-strain curve of the as deposited TiAlN film is also exhibited. A comparison of these curves reveals that on the one hand the superficial yield strength is significantly grown due to the conducted micro-blasting, even at the low pressure of 0.2 MPa; on the other hand, the rupture stress in both film cases remains practically invariant.

Furthermore, applying the same methodology presented in figure 4, nanoindentations at a larger load of 45 mN were conducted. These results were compared to results obtained from FEM calculations, to check whether using the film properties, shown in figure 5, a precise description of the coating deformation after micro-blasting can

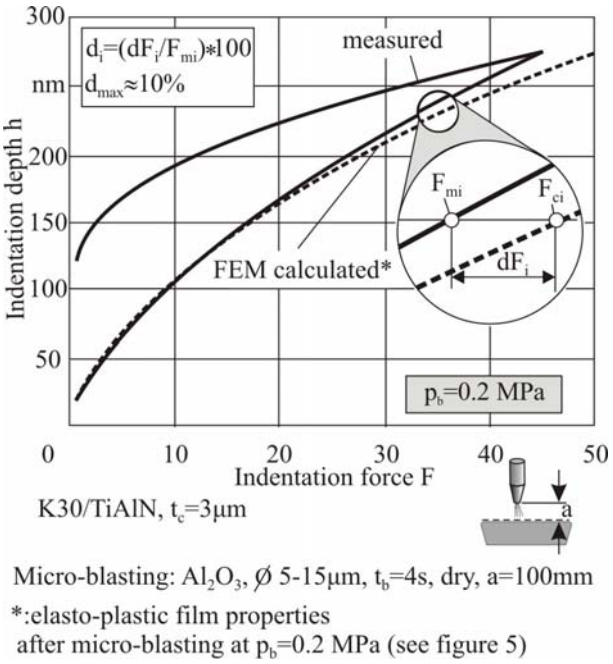

Figure 6. Deviations between measured and calculated nanoindentation forces versus the penetration depth, considering unique strength properties, after micro-blasting.

be achieved. As it can be observed in figure 6, the maximum deviation d_{max} between the measured and calculated indentation force versus the indentation depth amounts approximately to 10%, after the film's micro-blasting at 0.2 MPa. Similar results were obtained in the other pressure cases, thus indicating that the strength properties versus the film thickness are not unique after micro-blasting, i.e. a properties gradation exists.

To determine the occurring film mechanical properties gradation after micro-blasting, a computational–experimental method will be introduced. Among others, this method is based on a FEM simulation of the film deformation induced by blasting grains.

3. FEM-SUPPORTED DETERMINATION OF THE FILM MATERIAL DEFORMATION DURING AND AFTER MICRO-BLASTING

3.1 The developed FEM-model to describe the grain penetration

An axisymmetric FEM model of the semi-infinite layered half space was developed to simulate the grain penetration into the coating during micro-blasting, as it is demonstrated in figure 7 [8]. The plasticity model of the kinematic hardening rule was used because this model leads to a rapid convergence in the corresponding FEM calculations. The kinematic hardening assumes that the yield surface remains constant in size and the surface translates in

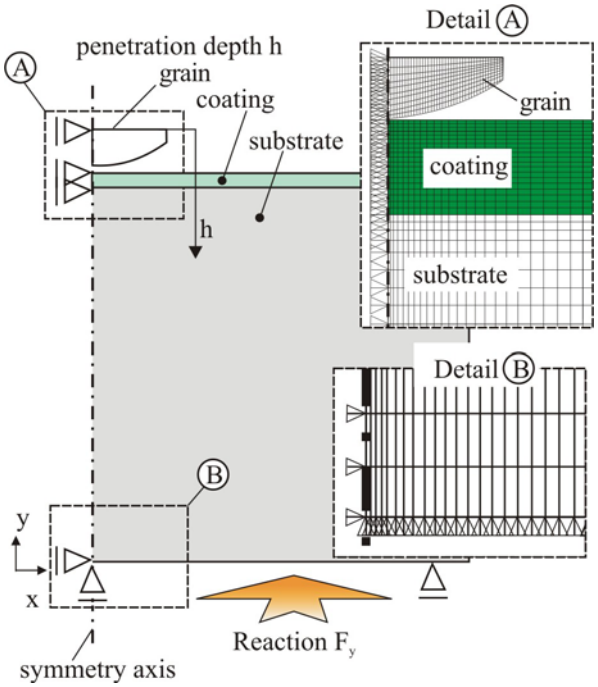

Figure 7. The developed FEM model to simulate the grain penetration during micro-blasting.

stress space with progressive yielding, whereas the Besseling model is applied, also called sub-layer or overlay model, to characterize the material behaviour [8,12,13]. The simulation software was the ANSYS 9.0 package and the corresponding mathematical relations are documented in [8]. In the conducted calculations, spherical Al_2O_3 grains with an average radius of 5 μm were considered. The boundary conditions and the finite elements discretisation network are explained in the same figure. Appropriate contact elements were used to describe the interface between the grain and the film surface. Moreover, the material properties, the coating thickness, the grain radius as well as the penetration depth are variable and changeable parameters. By this FEM model, the developed stress and strain fields during the grain penetration into the film material and the residual corresponding ones after the grain removal can be calculated. The developed reaction force Fy is equal to the grain load; this force and the stress-strain fields depend on the grain penetration depth. In this way, the load corresponding to a certain grain penetration depth and moreover the von Mises stress-strain fields during film loading and relaxation can be determined.

3.2 Characteristic calculation results

Characteristic results, obtained by the developed FEM model are exhibited in the upper left part of figure 8. The developed von Mises stresses at two reference points A and B at a grain penetration

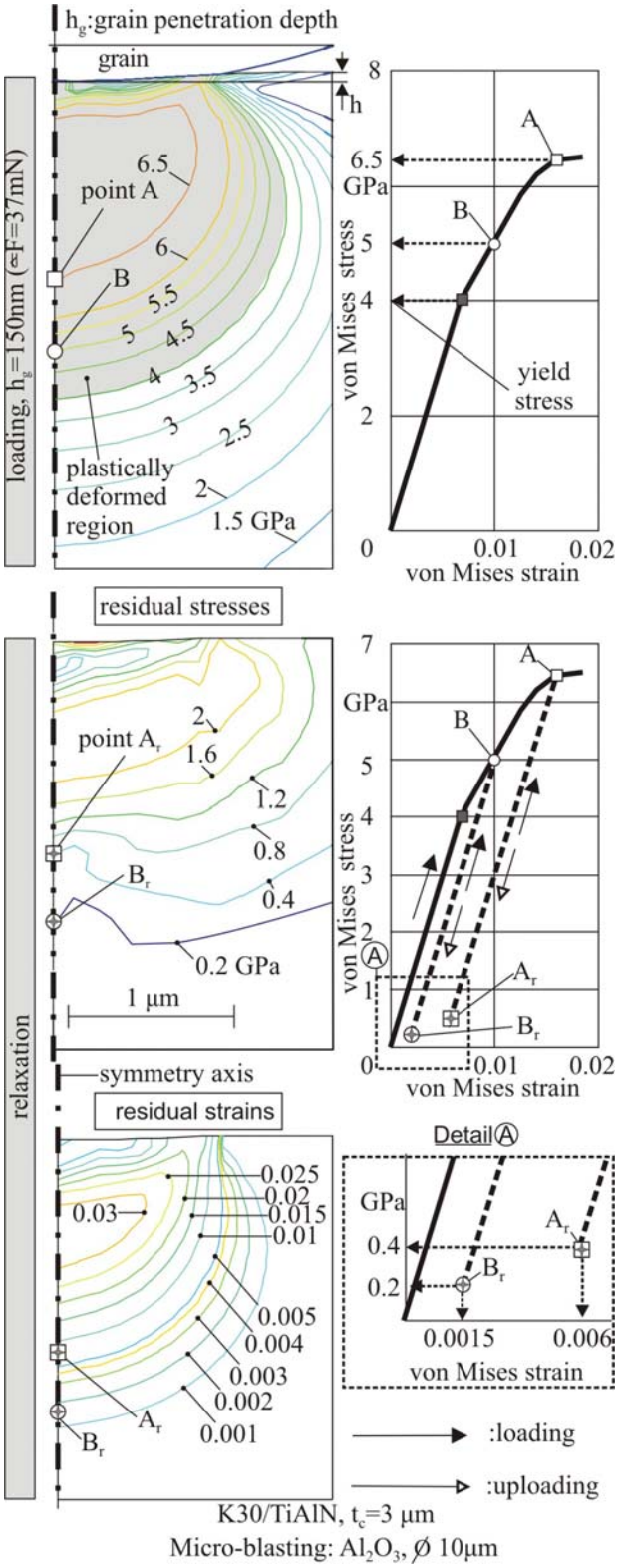

Figure 8. Von Mises stress and strain distributions in a TiAlN coating during and after micro-blasting.

depth h_g of 150 nm amount to 6.5 and 5 GPa respectively, both larger than the film yield stress of 4 GPa in the as deposited film case (see figure 3). Hence, the entire shaded film region is plastically deformed. Moreover, after the grain removal, i.e. during the film material relaxation, the remaining

plastic deformation leads to the residual stress and strain fields, exhibited in the lower left figure part.

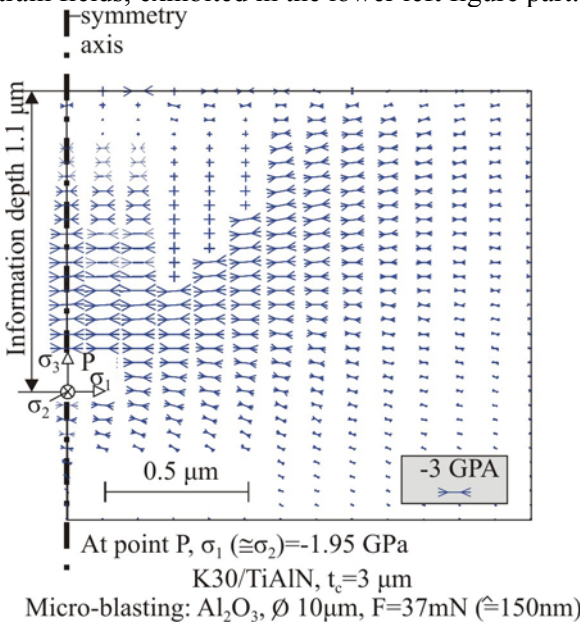

Figure 9. Principal stress σ_1 distributions in a TiAlN coating after micro-blasting.

When the coating is reloaded, for example through the penetration of a new blasting grain, the plastically deformed material behaves as possessing a yield strength greater than the pristine one. For example, in the regions of the points A and B, the actual yield stress amounts to 6.5 and 5 GPa respectively, as schematically explained in the right part of figure 8.

Additional significant data, which can be determined by the developed FEM model are the principal stresses related to the residual stress field. Associated principal stresses to the presented residual ones in figure 8 are exhibited in figure 9. The distribution of the residual principal stress in σ_1 direction is schematically shown. The displayed symbols indicate the direction and the size of the residual principal stress σ_1 at each point. Due to the axisymmetric FEM–model, the principal stresses at every point of the diagram in both σ_1 and σ_2 directions are equal. In this way the residual principal stresses σ_1 and σ_2 in the region of a reference point at a certain distance from the film surface can be predicted. For example at a specific depth from the film surface (information depth [14]) of ca 1.1 µm, both predicted principal stresses σ_1 and σ_2 in the region of the reference point P amount approximately to –1.95 GPa. These residual principal stresses represent simultaneously the stress changes in σ_1 and σ_2 directions after the coating micro-blasting, since in the related FEM-calculations, a free of residual stresses film material before micro-blasting was assumed. These stress changes can be compared to the corresponding ones, detected by XRD-measurements, as it will be further discussed. Based on these comparisons the grain penetration depth, which causes principal stress changes at the depth of a reference point after micro-blasting, equal to corresponding measured ones at the same point, can be determined.

4. RESIDUAL STRESSES AND GRAIN PENETRATION DEPTHS AT VARIOUS MICRO-BLASTING PRESSURES

4.1 XRD-measurement of residual stresses after micro-blasting at various pressures at a certain information depth

The residual stresses in the as deposited and in the micro-blasted TiAlN films at an information depth of 1.1 µm from the film surface, were measured by X-ray diffraction technique [1]. The measured results are demonstrated in figure 10 and reveal an impressive increase of the compressive residual stresses σ_{1r} and σ_{2r} from –0.4 and –0.7 GPa in the as deposited film case, up to –2.9 and –3.2 GPa respectively, after micro-blasting at a pressure of 0.6 MPa. Considering the as deposited residual stresses σ_{1r} and σ_{2r} as reference values, the corresponding changes $\Delta\sigma_{1r}$ and $\Delta\sigma_{2r}$ after micro-blasting at various pressures p_b can be determined. These changes are practically equal in both σ_1 and σ_2 directions at the same information depth of 1.1 µm, as it is exhibited in figure 10.

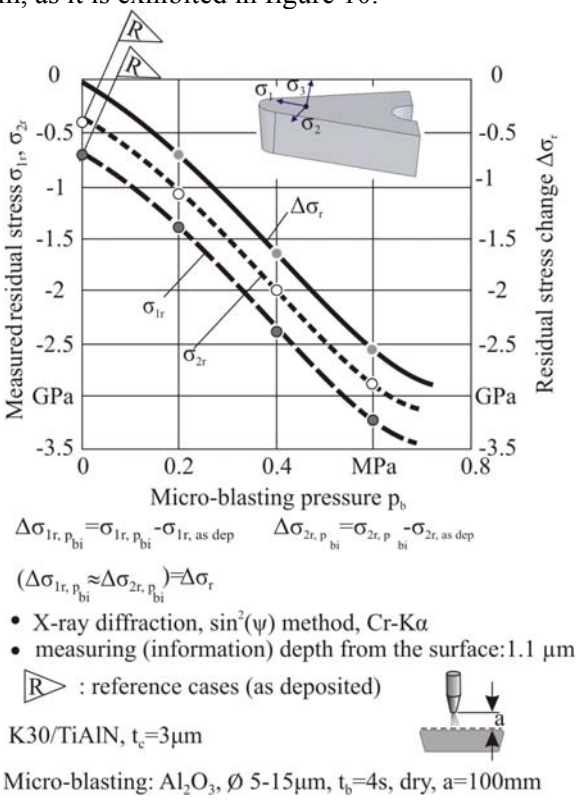

Figure 10. Occurring residual stresses and their changes in the investigated TIAlN films after micro-blasting at various pressures at an information depth of 1.1 µm.

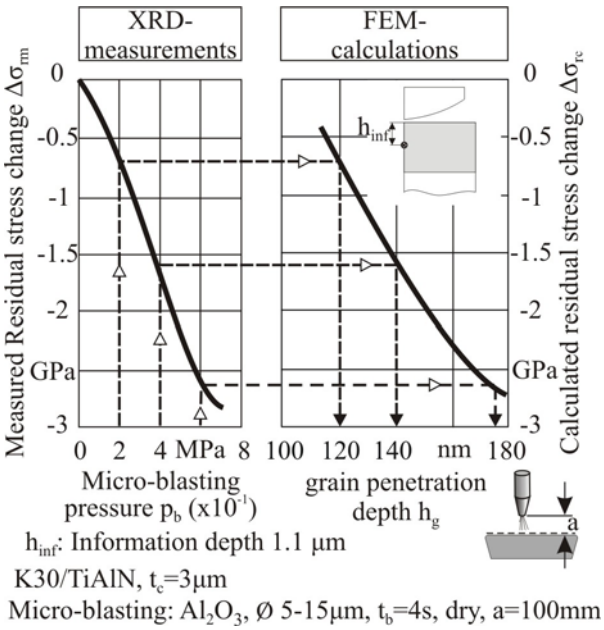

Figure 11. Determination of the required grain penetration depth to obtain residual stress changes after micro-blasting at various pressures in the coatings equal to the measured ones.

4.2 Determination of the grain penetration depth corresponding to a micro-blasting pressure

Based on the XRD-measurement results and on the FEM simulation of micro-blasting, the grain penetrations at various micro-blasting pressures can be predicted, as explained in figure 11. The residual stresses σ_{rm} after micro-blasting at various pressures at a certain information depth can be determined by XRD-measurements and their changes $\Delta\sigma_{rm}$ as well. The course of the measured changes $\Delta\sigma_{rm}$ versus the micro-blasting pressure p_b is illustrated in the diagram at the left part of figure 11. Moreover, these residual stress changes can be calculated in the same directions versus the grain penetration depth h_g (see right part of figure 11). In this way, at the same level of residual principal stress change $\Delta\sigma_r$ after micro-blasting, the grain penetration depths, which correspond to certain pressures can be predicted. In the examples of figure 11, the determination of the grain penetration depths, associated to the used micro-blasting pressures of 0.2, 0.4 and 0.6 MPa is demonstrated.

5. PREDICTION OF FILM STRENGTH PROPERTIES GRADATION AFTER MICRO-BLASTING AT VARIOUS PRESSURES

The von Mises stresses and plastic strains developed after micro-blasting along the grain impression symmetry axis depend on the distance from the coating surface and can be determined, as shown in figure 12; the shaded areas indicate film material plastic deformation. The applied grain penetration depth h_g at a micro-blasting pressure of 0.2 MPa amounts to 120 nm, according to figure 11. The determined residual stress and strain distributions along the impression symmetry axis are developed under every point of the film surface, since after a sufficient micro-blasting time, the grains deform uniformly the entire coating surface [1]. The yield strength of the untreated coating, which has unique strength properties, amounts to 4 GPa. Film regions, not plastically deformed during micro-blasting, possess the pristine yield stress of the as deposited material i.e. of 4 GPa. In turn, a plastically deformed region possesses a yield

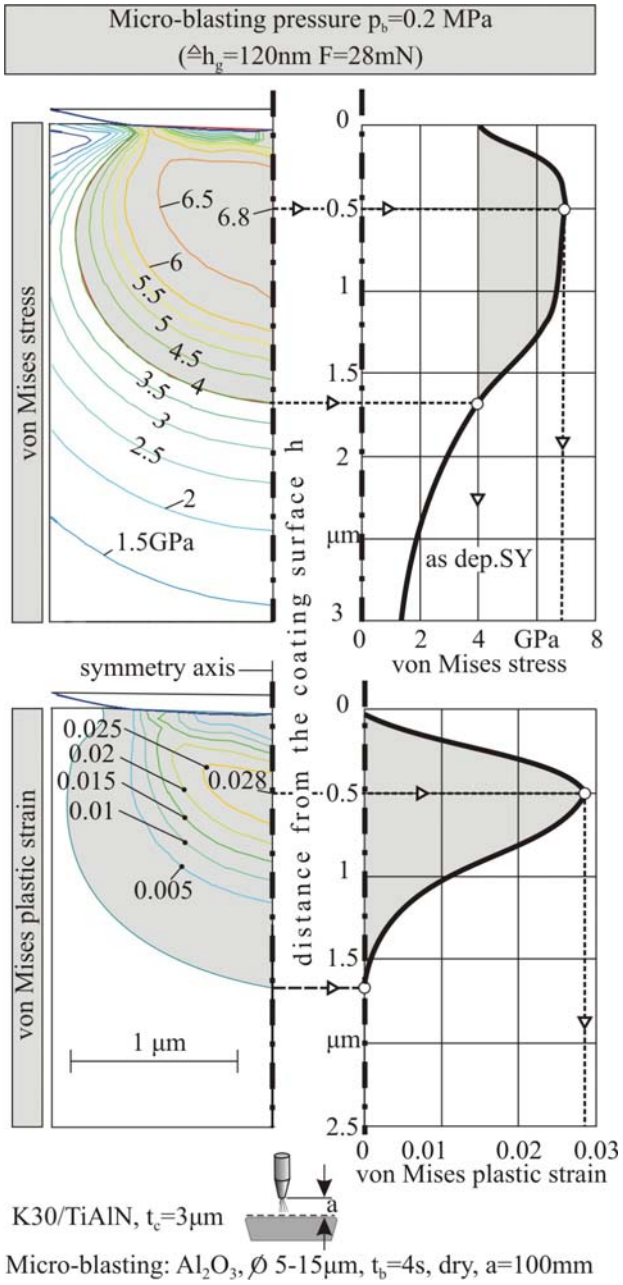

Figure 12. Calculated von Mises stress and plastic strain distributions in a TiAlN coating after micro-blasting.

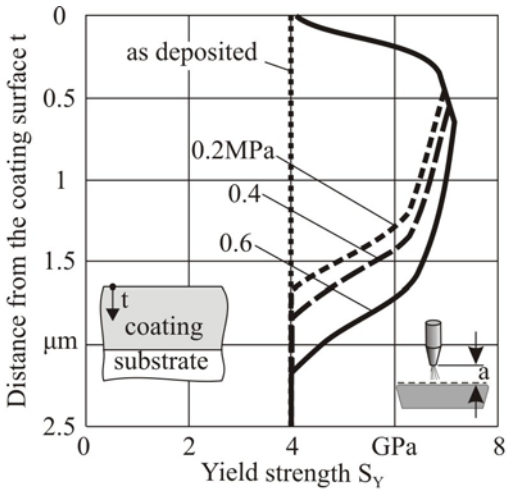

K30/TiAlN, t_c=3μm
Micro-blasting: Al_2O_3, Ø 5-15μm, t_b=4s, dry, a=100mm

Figure 13. Yield stress distributions in a TiAlN coating after micro-blasting at various pressures.

strength equal to the locally developed maximum von Mises stress, as explained in figure 8.

In the same way, the yield stress gradation versus the film thickness can be determined for all applied pressures, as it is exhibited in figure 13. According to the obtained results, a micro-blasting pressure growth leads to an enlargement of the plastically deformed film region. For example, at micro-basting pressures of 0.2, 0.4 and 0.6 MPa, the depth of this region increases approximately up to 1.6, 1.9 and 2.2 μm and the achieved maximum yield stress up to ca. 6.85, 6.95 and 7 GPa, respectively. It is notable that the film mechanical properties at a depth less than 0.5 μm remain practically unaffected by the micro-blasting pressure. Therefore, the nanoindentation results at a small indentation depth i.e. at the low load of 5mN were slightly influenced by the micro-blasting pressure magnitude (see figure 5).

6. VERIFICATION OF THE DETERMINED COATING STRENGTH PROPERTIES GRADATION BY NANOINENDATIONS AND FEM-CALCULATIONS

To check the validity of the determined film mechanical properties gradation, caused by micro-blasting, nanoindentations were conducted at a large indentation force of 45 mN. The measured courses of the indentation depth versus the indentation force of micro-blasted coatings at pressures of 0.2 and 0.6 MPa are displayed in figure 14. These results were compared to corresponding analytically determined ones, employing the developed FEM simulation of the nanoindentation. In these calculations, the coating thickness was approached by 30 material layers, each one with

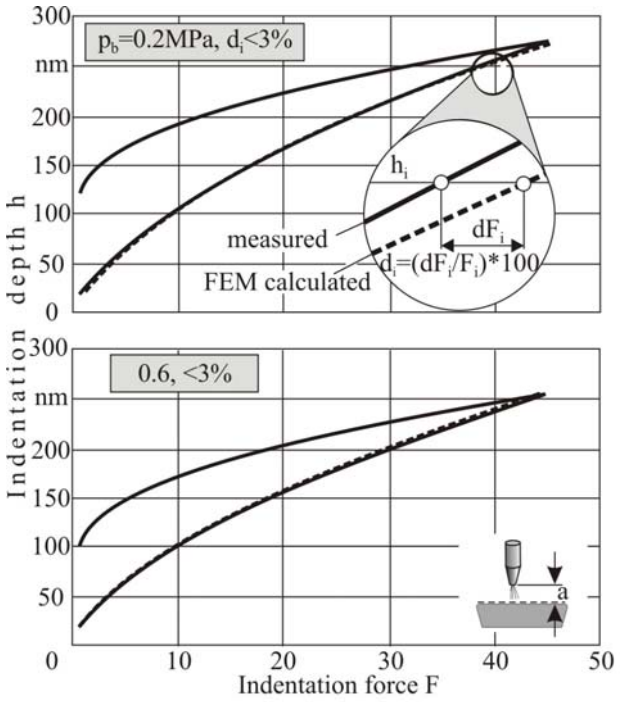

*:considering strength properties gradation, (30 layers) shown in figure13
Coating: TiAlN, t_c=3μm, Substrate: K30
Micro-blasting: Al_2O_3, Ø 5-15μm, t_b=4s, dry, a=100mm

Figure 14. Deviations between measured and calculated nanoindentation forces versus the penetration depth, in the case of micro-blasted films at 0.2 and 0.6 MPa, considering the determined properties gradation.

own yield strength, depending on its distance from the film surface, according to figure 13. The force deviations d_i between the measured and calculated forces versus the indentation depth are now less than ±3%, i.e. they are significantly smaller in comparison to the corresponding ones demonstrated in figure 6. Hence, considering the developed mechanical properties gradation after micro-blasting, the film material deformation can be accurately described.

7. NANOINDENTATIONS ON VARIOUSLY MICRO-BLASTED PVD FIMS

The TiAlN coated cemented carbides inserts were micro-blasted at various pressures and durations. In the upper diagram of figure 15, the maximum indentation depths at load of 15 mN on coated inserts, which were micro-blasted for duration of four seconds at various pressures, are displayed; further process parameters are monitored at the bottom of this figure. It is obvious that by increasing the micro-blasting pressure, a reduction of the maximum indentation depth occurs, thus improving the superficial hardness. The maximum indentation depth diminishing is almost linear versus micro-blasting pressure. Corresponding

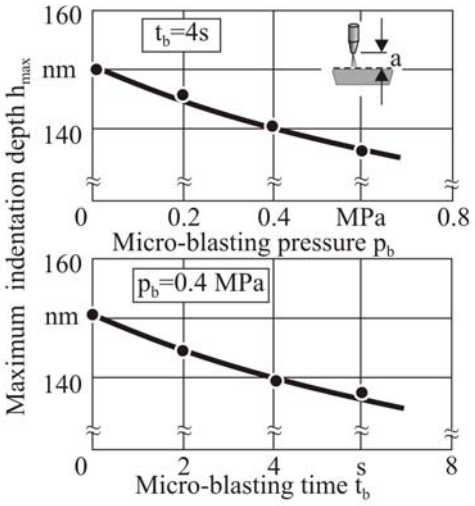

Figure 15. Nanoindentation results on coatings, micro-blasted at various pressures and durations.

investigations were conducted in the case of micro-blasted TiAlN films for various process durations, whereas the pressure was kept constant equal to 0.4 MPa. The reduction of the maxium indentation depth by increasing the micro blasting time is visible in the bottom diagram of figure 15. The decreasing of the maximum indentation depth versus the process time is approximately linear.

8. EFFECT OF MICRO-BLASTING PRESSURE AND DURATION ON COATING THICKNESS AND CUTTING EDGE GEOMETRY

The film thickness distribution on the rake and flank affects significantly the tool wear progress, as it is documented in the literature [15]. Thicker films on the tool rake compared to the flank and moreover, uniformly distributed films along the cutting edge, improve the cutting performance. Dependent on the applied conditions and grain data, abrasion may take place during micro-blasting leading to a coating thickness change in the cutting edge region. To investigate this effect, ball cratering tests were carried out on the coated rake and flank near the cutting edge after micro-blasting. A related imprint is exhibited at the top of figure 16. The imprint profiles were measured by white light scanning via the mentioned confocal device. Increased micro-blasting pressure and time led to a slight coating thickness reduction on the rake, while the coating thickness on the flank remains almost invariable (see related diagrams at the bottom of figure 16).

Moreover, to investigate the micro-blasting effects on the cutting edge roundness, white light

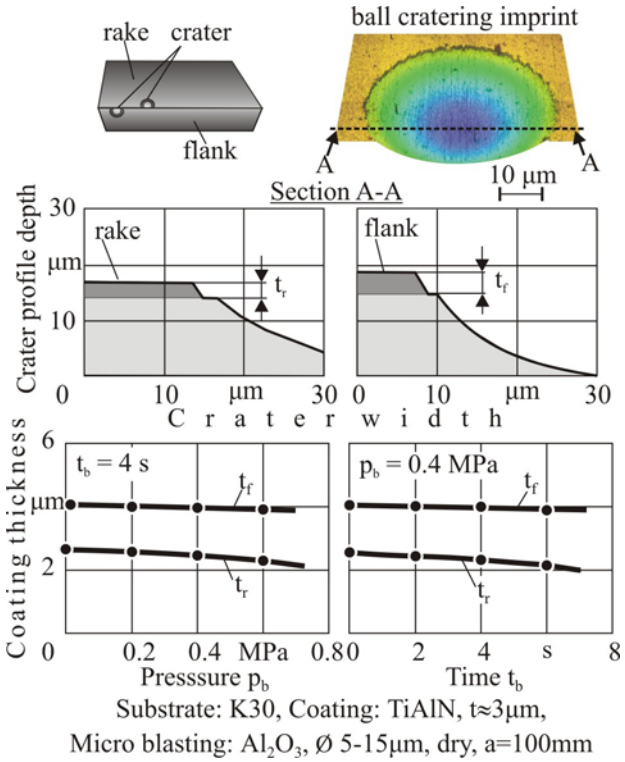

Figure 16. Ball cratering test on flank and rake surfaces.

scannings along the cutting edges of variously micro-blasted cutting inserts were conducted, as it is schematically explained at the top of figure 17. By these measurements, successive cross sections of the cutting edges were registered and the corresponding radii were determined. In this way, the average and the fluctuations of the cutting edge roundness after micro-blasting at various pressures were estimated and they are indicated in the corresponding diagrams of figure 17. The results

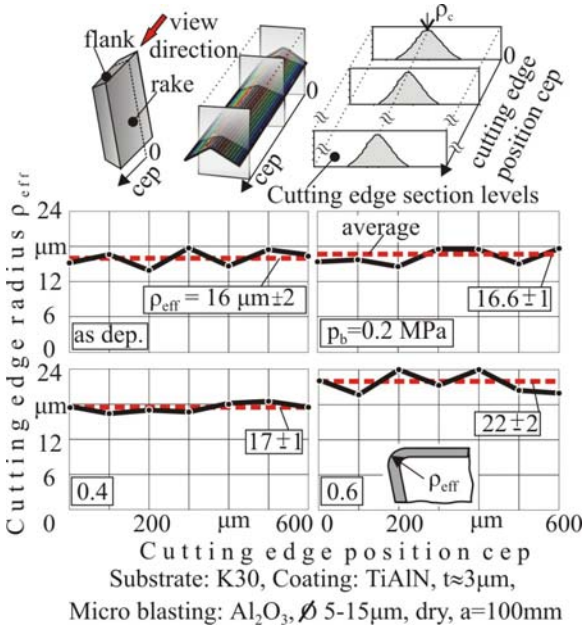

Figure 17. White light scanning measurements along the cutting edge.

revealed that by increasing the micro-blasting pressure an enlargement of the cutting edge radius develops.

Corresponding investigations were also conducted to capture the effect of micro-blasting time on the cutting edge roundness. In the diagrams of figure 18, cutting edge radii and their fluctuations versus the applied pressure and time are exhibited. The effect of micro blasting conditions on the cutting edge geometry is more intense, as pressure and time grow.

Considering the previous results, the coating thickness distributions along the cutting edge after micro-blasting at various pressures were analytically determined; the corresponding coated cutting edge geometries are monitored at the left part of figure 19. At process pressure of 0.4 MPa and up to a time of 6 seconds no substrate revelation occurred, as it can also be observed in the diagram at the top of this figure. In the case of micro-blasting pressure of 0.6 MPa, the occurring average minimum coating thickness on the cutting edge $t_{\rho min}$ amounts to 1.3 μm. Considering the cutting edge radius scatter (see diagram at the bottom of figure 19), $t_{\rho min}$ may diminish to zero, i.e. the substrate reveals and in this way the cutting performance is expected to significantly affected.

SEM micrographs and EDX microanalysis results, illustrated at the upper of figure 20, revealed a uniformly deposited film on the cutting edge without any substrate revelation. Moreover, substrate revelations on the cutting edges, micro-

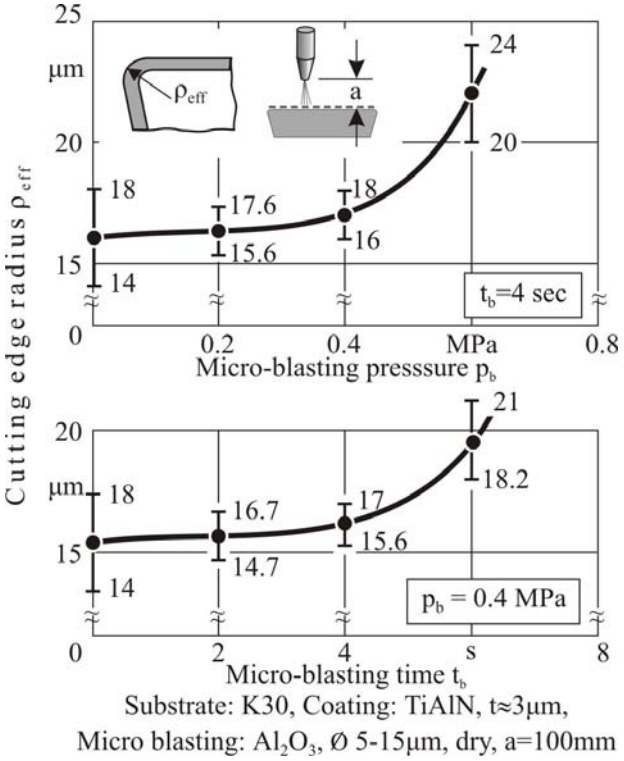

Figure 18. Average cutting edge radius versus the micro-blasting pressure and duration.

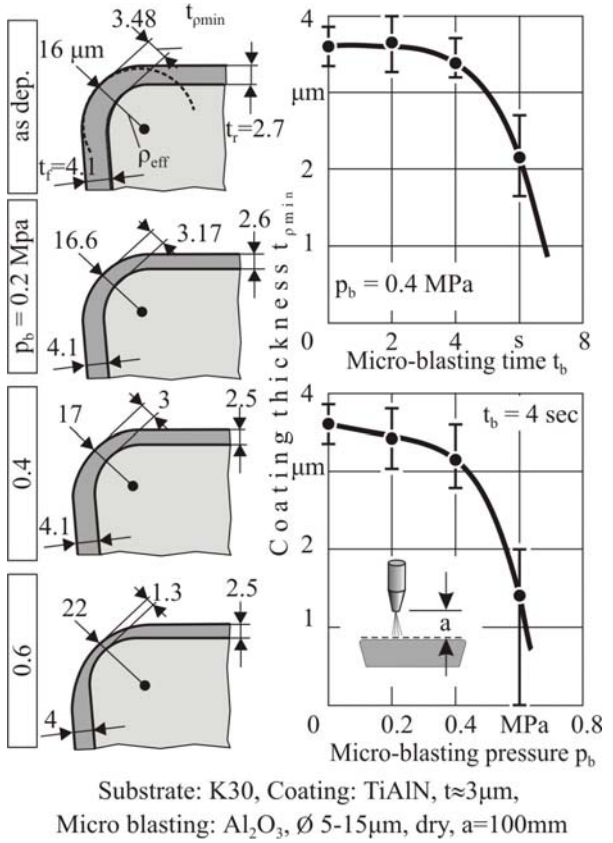

Figure 19. Characteristics geometries and minimum coating thickness $t_{\rho min}$ of the micro-blasted cutting edge.

blasted at pressures over ca. 0.4 MPa were recorded, in SEM micrographs and EDX microanalyses. Related characteristic results are illustrated in figure 20. The cutting edge roughness increases by the micro-blasting pressure growth, as it can be observed in the corresponding SEM

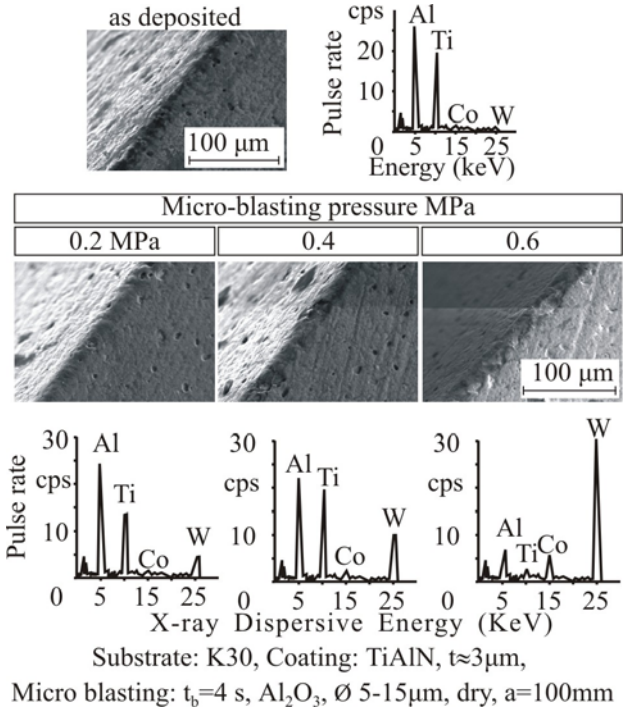

Figure 20. SEM micrographs and EDX microanalyses of the cutting edge.

micrographs. Furthermore, the EDX microanalyses, displayed at the lower part of figure 20, verify local coating removals at pressures larger than 0.4 MPa, since the substrate chemical elements W and Co were detected.

9. WEAR BEHAVIOR OF COATED TOOLS IN MILLING WITH MICRO-BLASTED FILMS AT VARIOUS CONDITIONS

To check the effect of micro-blasting conditions on the cutting performance of coated tools, milling investigations were conducted. The experiments were performed using a three-axis numerically controlled milling centre. The applied tool-workpiece system as well as the main characteristics of the undeformed chip geometry are illustrated at the top of figure 21. The flank wear development on coated inserts, which were micro-blasted at various pressures, is demonstrated at the bottom of figure 21. The micro-blasted tools at a pressure of 0.2 MPa exhibited the best cutting performance, reaching a tool life of 170.000 cuts up to a flank wear width of approximately 0.2 mm. A slight tool life reduction to 165.000 cuts up to the same flank wear occurred at a micro-blasting pressure of 0.4 MPa. The worst cutting performance appeared in the coated insert case subjected to micro-blasting at 0.6 MPa. Due to local coating removals and substrate revealings after micro-blasting at this pressure, as it is already demonstrated in figure 20, the thermal barrier at the cutting edge roundness is damaged and cutting heat flows into the tool, thus contributing significantly

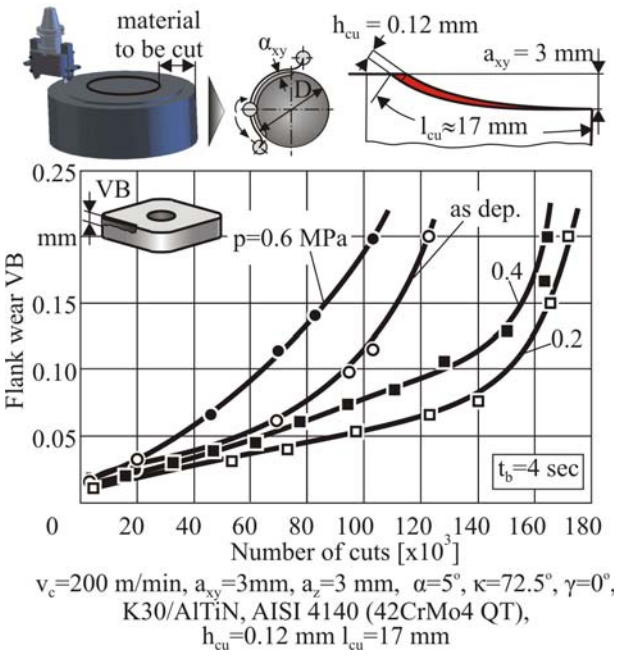

Figure 21. Flank wear development versus the number of cuts of tools micro-blasted at various pressures.

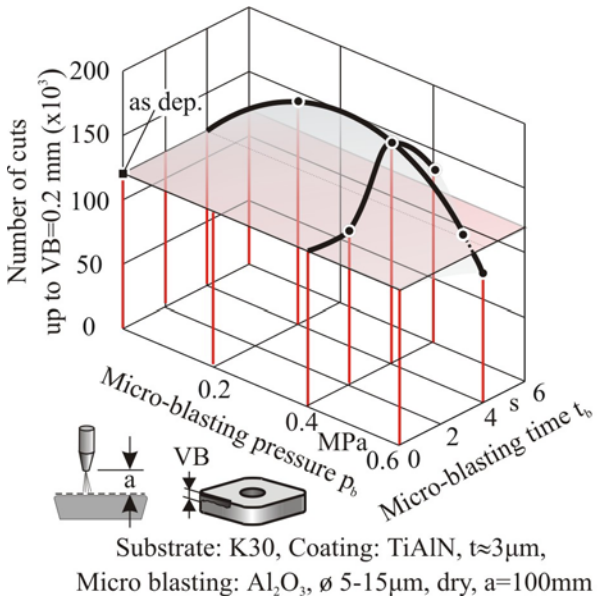

Figure 22. Overview of the achieved number of cuts dependent on micro-blasting pressure and time.

to cutting performance deterioration.

An overview of the achieved number of cuts up to a flank wear width of 0.2 mm, depending on the applied micro-blasting pressure and time is exhibited in figure 22. A significant increase of tool life is encountered by micro-blasting at pressures and process durations between 0.2 to 0.4 MPa and 3 to 6 s respectively. A further increase of the micro-blasting pressure or time deteriorates the coated tool cutting performance. Hence, the process parameters have to be appropriately selected for avoiding substrate revelation and thus tool life reduction.

10. DETERMINATION OF THERMAL AND MECHANICAL CUTTING LOADS BEFORE AND AFTER MICRO-BLASTING BY FEM-SUPPORTED CALCULATIONS

FEM calculations of the cutting process were conducted, using the DEFORM software for explaining the attained results [16,17]. In these calculations the actual geometries of the micro-blasted cutting edges, which are demonstrated at the top of figure 23, were considered. The film thickness on the transient area between flank and rake affects significantly the developed temperature field. In the case of micro-blasting at 0.6 MPa, the coating on the cutting edge may be removed, i.e. a zero thickness $t_{\rho min}$ occurs, thus leading to a significant increase of the maximum temperature up to 391 °C. The corresponding maximum temperature in the as deposited insert case amounts approximately to 253 °C. At the bottom of figure 23 the course of the maximum cutting temperature, at the transient area between flank and rake, versus

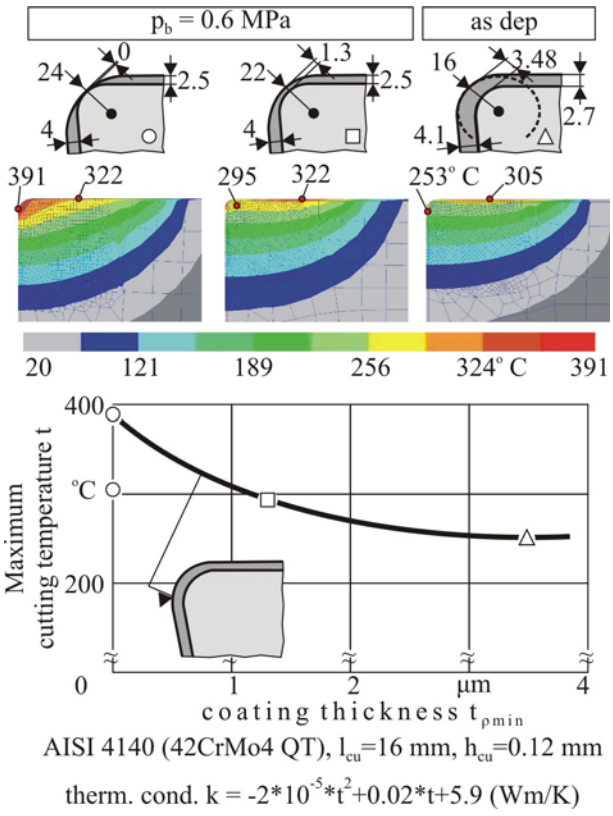

Figure 23. FEM calculations of temperature fields developed in the cutting edge region during milling.

the minimum coating thickness $t_{\rho min}$ is displayed. The larger the reduction of coating thickness, the more heat flows through the cutting edge roundness into the substrate.

The developed stresses fields in the cutting edge region are calculated by the ANSYS software package [8] (see figure 24). The cutting edge cross section geometries, which are already presented for various micro-blasting parameters at the top of figure 23, were considered in these FEM calculations. Moreover, the mechanical properties gradations along the coating thickness, before and after micro-blasting, illustrated in the right diagram at the top of figure 24, were taken into account [4]. Even though nowhere the tool coating is overstressed, the substrate of the micro-blasted tool at 0.6 MPa is loaded over its yield strength. Consequently, in this case the cutting edge with revealed substrate is highly thermally and mechanically loaded.

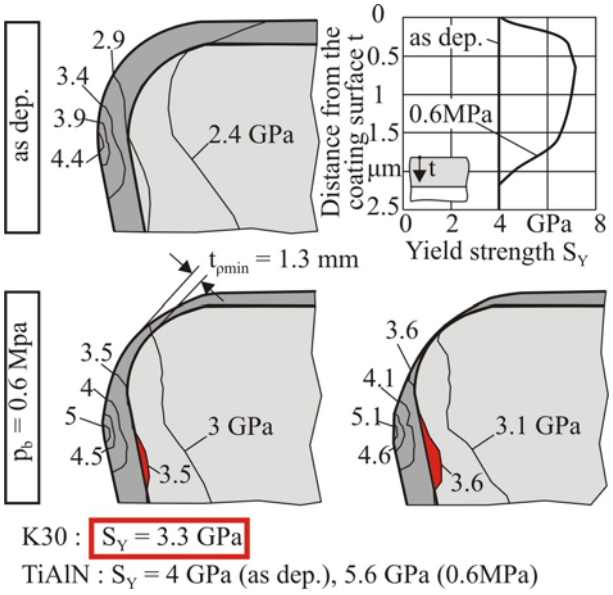

Figure 24. Stress distributions in the cutting edge region in various micro-blasted coated tool cases.

11. CONCLUSIONS

Micro-blasting on coated tools has been documented as an efficient method for improving cutting performance. In the paper, the effect of micro-blasting pressure and time on coated tool properties, cutting edge geometry and performance in milling was investigated and a novel method for enabling the determination of coating strength properties gradation after micro-blasting was introduced. This method is based on residual stress measurements obtained via the XRD technique and on a developed FEM-based analysis, describing the continuous penetration of individual grains into the coating material during and after micro-blasting. Abrasion mechanisms during micro-blasting may lead to coating thickness reduction and potential substrate revelation, thus causing coating and substrate thermal and mechanical loads growth. To counteract these effects, a comprehensive optimization of micro-blasting parameters pressure and time has to be performed.

REFERENCES

[1] E. Bouzakis, Steigerung der Leistungsfähigkeit PVD-beschichteter Hartmetallwerkzeuge durch Strahlbehandlung. Dissertation, RWTH Aachen, 2008.

[2] F. Klocke, T. Schroeder, E. Bouzakis, A. Klein, Manipulation of coating and subsurface properties in reconditioning of WC-Co carbide tools, Surface and Coatings Technology, 202, 1194-1198, 2007.

[3] D. M. Kenedy, J. Vahey, D. Hanney, Micro-shot blasting of machine tools for improving surface finish and reducing cutting forces in manufacturing, Material and Design, 26, 203-208, 2005.

[4] K.-D. Bouzakis, G. Skordaris, F. Klocke, E. Bouzakis, A FEM based analytical-experimental method for determining strength properties gradation in coatings after micro-blasting, Surface and Coatings Technology, DOI: 10.1016/j.surfcoat.2009.03.012.

[5] K.-D. Bouzakis, S. Gerardis, G. Skordaris, G. Katirtzoglou, S. Makrimallakis, F. Klocke, E. Bouzakis, E., Effect of dry micro-blasting on PVD-films properties, cutting edge geometry and tool life

in milling, 36th International Conference On Metallurgical Coatings And Thin Films ICMCTF 2009, 27 April-1 May 2009 San Diego, California, USA.

[6] G. Erkens, R. Cremer, T. Hamoudi, K.-D. Bouzakis, J. Mirisidis, S. Hadjiyiannis, G. Skordaris, A. Asimakopoulos, S. Kombogiannis, I. Anastopoulos, K. Efstathiou, Surface and Coatings Technology, Properties and performance of high aluminum containing (Ti,Al)N based supernitride coatings in innovative cutting applications, 177-178, 727-734, 2004.

[7] DEFORM 2D, 2007, Operational manual, DEFORM.

[8] Swanson Analysis System, INC., 2004, ANSYS user manual.

[9] K.–D. Bouzakis, N. Michailidis, S. Hadjiyiannis, G. Skordaris, G. Erkens, A continuous FEM simulation of the nanoindentation to determine actual indenter tip geometries, elastic-plastic material deformation laws and universal hardness, Zeitschrift für Metallkunde, 93, 862-869, 2002.

[10] K.-D. Bouzakis, G. Skordaris, S. Hadjiyiannis, A. Asimakopoulos, J. Mirisidis, N. Michailidis, G. Erkens, R. Cremer, F. Klocke, M. Kleinjans, Thin Solid Films, A nanoindentation based determination of internal stress alterations in PVD films and their cemented carbides substrates induced by recoating procedures and their effect on the cutting performance 447-448, 264-271, 2004.

[11] Rointan. F. Bunshah, Handbook of Hard Coatings, Noyes Publications / William Andrew Puplishing, LLC, Norwich, New York, U.S.A, 2001.

[12] J. L. Loubet, J. M. Georges, G. Meille, Vickers Indentation Curves of Elastoplastic Materials, Microindentation Techniques in Material Science and Engineering, ASTM STP 889, Philadephia (1986) 72-89.

[13] J.F. Besseling, E. Van Der Giessen, Mathematical Modelling of Inelastic Deformation, CHAPMAN & HALL, 1994, ISBN 0412452804.

[14] B. Denkena, B. Breidenstein, L. Gerdes, Residual stress distributions in uncoated, PVD coated and decoated carbides cutting tools, Proceedings of the 7th international "THE" Coatings in Manufacturing Engineering conference, ZITI Publication-Thessaloniki-Greece, 2008, pp. 29-38.

[15] K.-D. Bouzakis, S. Hadjiyiannis, G. Skordaris, I. Mirisidis, N. Michailidis G. Erkens, Wear development on cemented carbides inserts, coated with variable film thickness in the cutting wedge region, Surface and Coatings Technology, 188-189, 636-643, 2004.

[16] K.-D. Bouzakis, S. Gerardis, G. Katirtzoglou, S. Makrimallakis, N. Michailidis, E. Lili, Increasing tool life by adjusting the milling cutting conditions according to PVD films' properties, CIRP Annals-Manufacturing Technology, 57, 105-108, 2008.

[17] W. Kalss, A. Reiter, V. Derflinger, C. Gey, J.L. Endrino, Modern coatings in high performance cutting applications, International Journal of Refractory Metals and Hard Materials 24, 399-404, 2006.